Towards low timing phase noise operation in fiber lasers mode locked by graphene oxide and carbon nanotubes at 1.5 μm

Kan Wu,[1,*] Xiaohui Li,[2] Yonggang Wang,[3] Qi Jie Wang[2], Perry Ping Shum[2], and Jianping Chen[1]

[1]*State Key Laboratory of Advanced Optical Communication Systems and Networks, Department of Electronic Engineering, Shanghai Jiao Tong University, Shanghai 200240, China*

[2] *OPTIMUS, Centre of Excellence for Photonics, School of Electrical and Electronic Engineering, Nanyang Technological University, 50 Nanyang Ave., 639798, Singapore*

[3] *State Key Laboratory of Transient Optics and Photonics, Xi'an Institute of Optics and Precision Mechanics, Chinese Academy of Sciences, Xi'an 710119, China*

**kanwu@sjtu.edu.cn*

Abstract: We investigate the timing phase noise of fiber lasers mode locked by graphene oxide (GO) and carbon nanotubes (CNTs), respectively, integrated in a linear cavity fiber laser in the reflecting operation. Due to the shorter decay time of the GO and CNTs, weaker slow saturable absorber effects are expected and mode-locked lasers based on these two saturable absorbers exhibit low excess timing phase noise coupled from the laser intensity noise. Compared with a reference laser mode locked by semiconductor saturable absorber mirror (SESAM), GO based laser obtains a timing phase noise reduction of 7 dB at 1 kHz and a timing jitter reduction of 45% experimentally whereas CNTs based laser obtains a timing phase noise reduction of 3 dB and a timing jitter reduction of 29%. This finding suggests that saturable absorbers with short decay time have the potential for achieving mode locking operation with low timing phase noise, which is important for applications including frequency metrology, high-precision optical sampling, clock distribution and optical sensing.

OCIS codes: (160.4330) Nonlinear optical materials; (140.4050) Mode-locked lasers; (270.2500) Fluctuations, relaxations, and noise.

References and links

1. S. Y. Set, H. Yaguchi, Y. Tanaka, and M. Jablonski, "Laser mode locking using a saturable absorber incorporating carbon nanotubes," J. Lightwave Technol. **22**(1), 51–56 (2004).
2. M. A. Solodyankin, E. D. Obraztsova, A. S. Lobach, A. I. Chernov, A. V. Tausenev, V. I. Konov, and E. M. Dianov, "Mode-locked 1.93 microm thulium fiber laser with a carbon nanotube absorber," Opt. Lett. **33**(12), 1336–1338 (2008).
3. X.-H. Li, Y.-G. Wang, Y.-S. Wang, X.-H. Hu, W. Zhao, X.-L. Liu, J. Yu, C.-X. Gao, W. Zhang, and Z. Yang, "Wavelength-switchable and wavelength-tunable all-normal-dispersion mode-locked Yb-doped fiber laser based on single-walled carbon nanotube wall paper absorber," IEEE Photon. J. **4**(1), 234–241 (2012).
4. A. Martinez, K. Fuse, and S. Yamashita, "Mechanical exfoliation of graphene for the passive mode-locking of fiber lasers," Appl. Phys. Lett. **99**(12), 121107 (2011).
5. S. Yamashita, Y. Inoue, S. Maruyama, Y. Murakami, H. Yaguchi, M. Jablonski, and S. Y. Set, "Saturable absorbers incorporating carbon nanotubes directly synthesized onto substrates and fibers and their application to mode-locked fiber lasers," Opt. Lett. **29**(14), 1581–1583 (2004).
6. A. Tausenev, E. Obraztsova, A. Lobach, A. Chernov, V. Konov, P. Kryukov, A. Konyashchenko, and E. Dianov, "177 fs erbium-doped fiber laser mode locked with a cellulose polymer film containing single-wall carbon nanotubes," Appl. Phys. Lett. **92**(17), 171113 (2008).
7. Y.-W. Song, S. Yamashita, C. S. Goh, and S. Y. Set, "Passively mode-locked lasers with 17.2-GHz fundamental-mode repetition rate pulsed by carbon nanotubes," Opt. Lett. **32**(4), 430–432 (2007).

#224095 - $15.00 USD Received 29 Sep 2014; revised 7 Nov 2014; accepted 10 Nov 2014; published 9 Jan 2015

8. K. Jiang, S. Fu, P. Shum, and C. Lin, "A wavelength-switchable passively harmonically mode-locked fiber laser with low pumping threshold using single-walled carbon nanotubes," IEEE Photon. Technol. Lett. **22**(11), 754–756 (2010).
9. K. Wu, J. H. Wong, P. Shum, D. R. C. S. Lim, V. K. H. Wong, K. E. K. Lee, J. Chen, and E. D. Obraztsova, "Timing-jitter reduction of passively mode-locked fiber laser with a carbon nanotube saturable absorber by optimization of cavity loss," Opt. Lett. **35**(7), 1085–1087 (2010).
10. K. Wu, J. H. Wong, P. Shum, S. Fu, C. Ouyang, H. Wang, E. J. R. Kelleher, A. I. Chernov, E. D. Obraztsova, and J. Chen, "Nonlinear coupling of relative intensity noise from pump to a fiber ring laser mode-locked with carbon nanotubes," Opt. Express **18**(16), 16663–16670 (2010).
11. F. Bonaccorso, Z. Sun, T. Hasan, and A. C. Ferrari, "Graphene photonics and optoelectronics," Nat. Photonics **4**(9), 611–622 (2010).
12. Z. Sun, T. Hasan, F. Torrisi, D. Popa, G. Privitera, F. Wang, F. Bonaccorso, D. M. Basko, and A. C. Ferrari, "Graphene mode-locked ultrafast laser," ACS Nano **4**(2), 803–810 (2010).
13. Q. Bao, H. Zhang, Y. Wang, Z. Ni, Y. Yan, Z. X. Shen, K. P. Loh, and D. Y. Tang, "Atomic-layer graphene as a saturable absorber for ultrafast pulsed lasers," Adv. Funct. Mater. **19**(19), 3077–3083 (2009).
14. H. Zhang, D. Tang, R. J. Knize, L. Zhao, Q. Bao, and K. P. Loh, "Graphene mode locked, wavelength-tunable, dissipative soliton fiber laser," Appl. Phys. Lett. **96**(11), 111112 (2010).
15. A. Martinez and Z. Sun, "Nanotube and graphene saturable absorbers for fibre lasers," Nat. Photonics **7**(11), 842–845 (2013).
16. M. N. Cizmeciyan, J. W. Kim, S. Bae, B. H. Hong, F. Rotermund, and A. Sennaroglu, "Graphene mode-locked femtosecond Cr:ZnSe laser at 2500 nm," Opt. Lett. **38**(3), 341–343 (2013).
17. M. Zhang, E. J. R. Kelleher, F. Torrisi, Z. Sun, T. Hasan, D. Popa, F. Wang, A. C. Ferrari, S. V. Popov, and J. R. Taylor, "Tm-doped fiber laser mode-locked by graphene-polymer composite," Opt. Express **20**(22), 25077–25084 (2012).
18. J. Ma, G. Q. Xie, P. Lv, W. L. Gao, P. Yuan, L. J. Qian, H. H. Yu, H. J. Zhang, J. Y. Wang, and D. Y. Tang, "Graphene mode-locked femtosecond laser at 2 μm wavelength," Opt. Lett. **37**(11), 2085–2087 (2012).
19. D. Popa, Z. Sun, F. Torrisi, T. Hasan, F. Wang, and A. C. Ferrari, "Sub 200 fs pulse generation from a graphene mode-locked fiber laser," Appl. Phys. Lett. **97**(20), 203106 (2010).
20. I. H. Baek, H. W. Lee, S. Bae, B. H. Hong, Y. H. Ahn, D.-I. Yeom, and F. Rotermund, "Efficient mode-locking of sub-70-fs Ti: sapphire laser by graphene saturable absorber," Appl. Phys. Express **5**(3), 032701 (2012).
21. A. Martinez, K. Fuse, B. Xu, and S. Yamashita, "Optical deposition of graphene and carbon nanotubes in a fiber ferrule for passive mode-locked lasing," Opt. Express **18**(22), 23054–23061 (2010).
22. Y.-W. Song, S.-Y. Jang, W.-S. Han, and M.-K. Bae, "Graphene mode-lockers for fiber lasers functioned with evanescent field interaction," Appl. Phys. Lett. **96**(5), 051122 (2010).
23. Z. Zheng, C. Zhao, S. Lu, Y. Chen, Y. Li, H. Zhang, and S. Wen, "Microwave and optical saturable absorption in graphene," Opt. Express **20**(21), 23201–23214 (2012).
24. H. Zhang, S. Virally, Q. Bao, L. K. Ping, S. Massar, N. Godbout, and P. Kockaert, "Z-scan measurement of the nonlinear refractive index of graphene," Opt. Lett. **37**(11), 1856–1858 (2012).
25. Z. Luo, M. Zhou, J. Weng, G. Huang, H. Xu, C. Ye, and Z. Cai, "Graphene-based passively Q-switched dual-wavelength erbium-doped fiber laser," Opt. Lett. **35**(21), 3709–3711 (2010).
26. J. Liu, J. Xu, and P. Wang, "Graphene-based passively Q-switched 2μm thulium-doped fiber laser," Opt. Commun. **285**(24), 5319–5322 (2012).
27. G. Sobon, J. Sotor, J. Jagiello, R. Kozinski, M. Zdrojek, M. Holdynski, P. Paletko, J. Boguslawski, L. Lipinska, and K. M. Abramski, "Graphene Oxide vs. Reduced Graphene Oxide as saturable absorbers for Er-doped passively mode-locked fiber laser," Opt. Express **20**(17), 19463–19473 (2012).
28. Z.-B. Liu, X. He, and D. N. Wang, "Passively mode-locked fiber laser based on a hollow-core photonic crystal fiber filled with few-layered graphene oxide solution," Opt. Lett. **36**(16), 3024–3026 (2011).
29. J. Xu, J. Liu, S. Wu, Q.-H. Yang, and P. Wang, "Graphene oxide mode-locked femtosecond erbium-doped fiber lasers," Opt. Express **20**(14), 15474–15480 (2012).
30. M. Jung, J. Koo, P. Debnath, Y.-W. Song, and J. H. Lee, "A mode-locked 1.91 μm fiber laser based on interaction between graphene oxide and evanescent field," Appl. Phys. Express **5**(11), 112702 (2012).
31. X. Li, Y. Wang, Y. Wang, Y. Zhang, K. Wu, P. P. Shum, X. Yu, Y. Zhang, and Q. Wang, "All-normal-dispersion passively mode-locked Yb-doped fiber ring laser based on a graphene oxide saturable absorber," Laser Phys. Lett. **10**(7), 075108 (2013).
32. X. Li, Y. Tang, Z. Yan, Y. Wang, B. Meng, G. Liang, H. Sun, X. Yu, Y. Zhang, X. Cheng, and Q. J. Wang, "Broadband saturable absorption of graphene oxide thin film and its application in pulsed fiber lasers," IEEE J. Quantum Electron. **20**, 1–7 (2014).
33. S. Lu, C. Zhao, Y. Zou, S. Chen, Y. Chen, Y. Li, H. Zhang, S. Wen, and D. Tang, "Third order nonlinear optical property of Bi_2Se_3," Opt. Express **21**(2), 2072–2082 (2013).
34. C. Zhao, H. Zhang, X. Qi, Y. Chen, Z. Wang, S. Wen, and D. Tang, "Ultra-short pulse generation by a topological insulator based saturable absorber," Appl. Phys. Lett. **101**(21), 211106 (2012).
35. S. Chen, C. Zhao, Y. Li, H. Huang, S. Lu, H. Zhang, and S. Wen, "Broadband optical and microwave nonlinear response in topological insulator," Opt. Mater. Express **4**(4), 587–596 (2014).
36. J. Sotor, G. Sobon, W. Macherzynski, P. Paletko, K. Grodecki, and K. M. Abramski, "Mode-locking in Er-doped fiber laser based on mechanically exfoliated Sb2Te3 saturable absorber," Opt. Mater. Express **4**(1), 1–6 (2014).

#224095 - $15.00 USD Received 29 Sep 2014; revised 7 Nov 2014; accepted 10 Nov 2014; published 9 Jan 2015

37. J. Sotor, G. Sobon, K. Grodecki, and K. Abramski, "Mode-locked erbium-doped fiber laser based on evanescent field interaction with Sb2Te3 topological insulator," Appl. Phys. Lett. **104**(25), 251112 (2014).
38. H. Yu, H. Zhang, Y. Wang, C. Zhao, B. Wang, S. Wen, H. Zhang, and J. Wang, "Topological insulator as an optical modulator for pulsed solid-state lasers," Laser and Photonics Reviews **7**(6), L77–L83 (2013).
39. J. Lee, J. Koo, Y.-M. Jhon, and J. H. Lee, "A femtosecond pulse erbium fiber laser incorporating a saturable absorber based on bulk-structured Bi_2Te_3 topological insulator," Opt. Express **22**(5), 6165–6173 (2014).
40. M. Jung, J. Lee, J. Koo, J. Park, Y.-W. Song, K. Lee, S. Lee, and J. H. Lee, "A femtosecond pulse fiber laser at 1935 nm using a bulk-structured Bi_2Te_3 topological insulator," Opt. Express **22**(7), 7865–7874 (2014).
41. Z.-C. Luo, M. Liu, H. Liu, X.-W. Zheng, A.-P. Luo, C.-J. Zhao, H. Zhang, S.-C. Wen, and W.-C. Xu, "2 GHz passively harmonic mode-locked fiber laser by a microfiber-based topological insulator saturable absorber," Opt. Lett. **38**(24), 5212–5215 (2013).
42. Z. Luo, Y. Huang, J. Weng, H. Cheng, Z. Lin, B. Xu, Z. Cai, and H. Xu, "1.06 μm Q-switched ytterbium-doped fiber laser using few-layer topological insulator Bi_2Se_3 as a saturable absorber," Opt. Express **21**(24), 29516–29522 (2013).
43. H. Zhang, S. B. Lu, J. Zheng, J. Du, S. C. Wen, D. Y. Tang, and K. P. Loh, "Molybdenum disulfide (MoS_2) as a broadband saturable absorber for ultra-fast photonics," Opt. Express **22**(6), 7249–7260 (2014).
44. U. Keller, "Recent developments in compact ultrafast lasers," Nature **424**(6950), 831–838 (2003).
45. D. H. Sutter, G. Steinmeyer, L. Gallmann, N. Matuschek, F. Morier-Genoud, U. Keller, V. Scheuer, G. Angelow, and T. Tschudi, "Semiconductor saturable-absorber mirror assisted Kerr-lens mode-locked Ti:sapphire laser producing pulses in the two-cycle regime," Opt. Lett. **24**(9), 631–633 (1999).
46. Y. Wang, S. Wang, J. Luo, Y. Ge, L. Li, D. Tang, D. Shen, S. Zhang, F. W. Wise, and L. Zhao, "Vector Soliton Generation in a Tm Fiber Laser," IEEE Photon. Technol. Lett. **26**(8), 769–772 (2014).
47. J. L. Luo, Y. Q. Ge, D. Y. Tang, S. M. Zhang, D. Y. Shen, and L. M. Zhao, "Mechanism of spectrum moving, narrowing, broadening, and wavelength switching of dissipative solitons in all-normal-dispersion Yb-fiber lasers," IEEE Photon. J. **6**(1), 1–8 (2014).
48. J. Zhou, S. Fu, F. Luan, J. H. Wong, S. Aditya, P. P. Shum, and K. E. K. Lee, "Tunable multi-tap bandpass microwave photonic filter using a windowed Fabry-Perot filter-based multi-wavelength tunable laser," J. Lightw. Tech. **29**, 3381–3386 (2011).
49. H. A. Haus and A. Mecozzi, "Noise of mode-locked lasers," IEEE J. Quantum Electr. **29**(3), 983–996 (1993).
50. R. Paschotta, "Noise of mode-locked lasers (Part I): numerical model," Appl. Phys. B **79**(2), 153–162 (2004).
51. R. Paschotta, "Noise of mode-locked lasers (Part II): timing jitter and other fluctuations," Appl. Phys. B **79**(2), 163–173 (2004).
52. K. Wu, P. P. Shum, S. Aditya, C. Ouyang, J. H. Wong, H. Q. Lam, and K. E. K. Lee, "Noise conversion from pump to the passively mode-locked fiber lasers at 1.5 μm," Opt. Lett. **37**(11), 1901–1903 (2012).
53. D. Li, U. Demirbas, A. Benedick, A. Sennaroglu, J. G. Fujimoto, and F. X. Kärtner, "Attosecond timing jitter pulse trains from semiconductor saturable absorber mode-locked Cr:LiSAF lasers," Opt. Express **20**(21), 23422–23435 (2012).
54. C. Kim, S. Bae, K. Kieu, and J. Kim, "Sub-femtosecond timing jitter, all-fiber, CNT-mode-locked Er-laser at telecom wavelength," Opt. Express **21**(22), 26533–26541 (2013).
55. T. D. Mulder, R. P. Scott, and B. H. Kolner, "Amplitude and envelope phase noise of a modelocked laser predicted from its noise transfer function and the pump noise power spectrum," Opt. Express **16**(18), 14186–14191 (2008).
56. F. X. Kurtner, J. A. der Au, and U. Keller, "Mode-locking with slow and fast saturable absorbers-what's the difference?" IEEE J. Quantum Electron. **4**(2), 159–168 (1998).
57. X. Zhao, Z.-B. Liu, W.-B. Yan, Y. Wu, X.-L. Zhang, Y. Chen, and J.-G. Tian, "Ultrafast carrier dynamics and saturable absorption of solution-processable few-layered graphene oxide," Appl. Phys. Lett. **98**(12), 121905 (2011).
58. Y.-C. Chen, N. Raravikar, L. Schadler, P. Ajayan, Y.-P. Zhao, T.-M. Lu, G.-C. Wang, and X.-C. Zhang, "Ultrafast optical switching properties of single-wall carbon nanotube polymer composites at 1.55 μm," Appl. Phys. Lett. **81**(6), 975–977 (2002).
59. BATOP, "SAM-1550-9-2ps datasheet" (2011), retrieved *http://www.batop.de/products/saturable-absorber/saturable-absorber-mirror/saturable-absorber-mirror-1550nm.html*.
60. H. Byun, M. Y. Sander, A. Motamedi, H. Shen, G. S. Petrich, L. A. Kolodziejski, E. P. Ippen, and F. X. Kärtner, "Compact, stable 1 GHz femtosecond Er-doped fiber lasers," Appl. Opt. **49**(29), 5577–5582 (2010).
61. C. Manzoni, A. Gambetta, E. Menna, M. Meneghetti, G. Lanzani, and G. Cerullo, "Intersubband exciton relaxation dynamics in single-walled carbon nanotubes," Phys. Rev. Lett. **94**(20), 207401 (2005).

1. Introduction

Novel materials have emerged in recent years as versatile saturable absorbers (SAs) for mode-locked lasers. By engineering the synthesis process of the materials, different SA properties can be obtained. Carbon nanotubes (CNTs) have been firstly demonstrated for their flexibility in mode locking operation with various center wavelengths [1–3], material preparation methods [4–6], laser repetition rate [7, 8] and laser noise properties [9, 10]. Graphene as

#224095 - $15.00 USD Received 29 Sep 2014; revised 7 Nov 2014; accepted 10 Nov 2014; published 9 Jan 2015

another important SA has been reported for achieving mode locking with different operation wavelengths [11–18], high pulse energy [19,20] and different material incorporating method [21, 22]. The nonlinear properties and Q-switched operation of graphene have also been investigated [23–26]. Similar findings in graphene oxide (GO) have been demonstrated at different center wavelengths [27–30] and in different laser operation modes [31, 32]. Topological insulators have been proved as a new type of SA. Their 2-dimensional (2D) structures show much similarities with graphene and experimental results have been reported in the lasers incorporating their nonlinear properties [33–35], flexible material utilization [36–38], narrow-pulse-width operations [39, 40], high-repetition-rate mode locking [41] and Q-switched operation [42]. Very recently, transition metal dichalcogenides MoS_2 has been found to have the saturable absorption characteristics and its broadband mode locking operation has been achieved [43]. Meanwhile, there is another well-known SA, semiconductor saturable absorber mirror (SESAM), which exhibits excellent engineering flexibility for different SA parameters and has been proved as a significant success in mode locking operations [44–47].

For applications such as frequency metrology, optical sampling, clock distribution and optical sensing, laser timing phase noise and timing jitter are key parameters to achieve high precision [48]. The timing phase noise model of mode-locked lasers has been developed [49–51] and experimental investigations of noise coupling have been reported [10, 52]. Mode-locked lasers with low timing jitter have also demonstrated [53, 54]. However, the role of SAs on the timing phase noise of the mode-locked lasers has not been studied yet. Therefore it is meaningful to understand how different SAs affect the laser noise.

In this paper, from the view of timing phase noise of the mode-locked lasers, we investigate the noise properties of the fiber lasers operating at 1.5 μm mode locked by GO and single wall CNTs and compare them with a reference laser mode locked by SESAM (denoted as GO laser, CNT laser and SESAM laser, respectively). All three types of SAs share exactly the same linear laser cavity so that the influence of the laser cavity difference can be excluded as much as possible in the comparison. It is found that timing phase noises of three lasers are all dominated by the noise coupled from the laser relative intensity noise (RIN) due to the slow saturable absorber (SSA) effect, i.e., the laser RIN couples to the laser timing phase noise due to the time dependent response of the SA. Timing phase noise spectrum can be predicted through the measured laser RIN spectrum and noise conversion ratios. Moreover, compared with the SESAM laser, the GO laser and the CNT laser exhibit lower timing phase noise and timing jitter due to the smaller SA decay time and weaker SSA effect. 7-dB improvement in the timing phase noise spectrum and 45% timing jitter reduction is observed in the GO laser. And a 3-dB improvement in the timing phase noise spectrum and 29% timing jitter reduction are observed in the CNT laser. This result indicates that SAs with smaller decay time have the potential to achieve mode locking with low timing phase noise.

2. Preparation of GO and CNT saturable absorbers

GO and single wall CNTs are embedded in PVA thin films for the experiments. The preparation of GO-PVA and CNT-PVA thin films are described as follows: GO sheets are fabricated by ultrasonic agitation after chemical oxidation of graphite and then dispersed in water. Single wall CNTs are dispersed in sodium dodecyl sulfate (SDS) aqueous solution by ultrasonic process. PVA is then added to the GO or CNT solutions, heated to 90 degrees and further mixed with CNT or GO by ultrasonic process. The prepared solutions are then poured into polystyrene cells. Part of the solution is adhered to the polystyrene cell wall due to the high viscosity to the cell wall. After evaporation process, GO-PVA or CNT-PVA thin films are formed and attached to the cell wall, which can be easily stripped off by tweezers. These SA thin films are then cut into small pieces and placed on the fiber end for experimental use. The thickness of GO-PVA and CNT-PVA thin films is between 35 ~50 μm characterized by the scanning electron microscope (SEM). The whole process is summarized in Fig. 1.

#224095 - $15.00 USD Received 29 Sep 2014; revised 7 Nov 2014; accepted 10 Nov 2014; published 9 Jan 2015

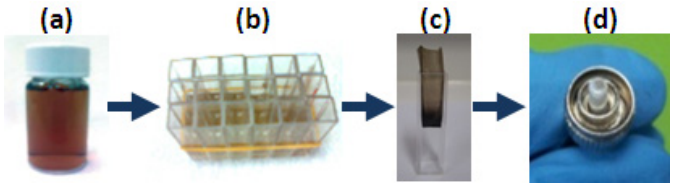

Fig. 1. Preparation of GO-PVA and CNT-PVA thin film SAs (a) GO and CNT dispersed solution; (b) polystyrene cells filled with solutions; (c) thin film stripped off the cell wall after heating and evaporation process; (d) small piece of thin film SA on a fiber end.

The saturable absorption of the GO-PVA and CNT-PVA thin films is characterized by a homemade mode-locked laser operating at 1560 nm as shown in Fig. 2. It can be seen that GO-PVA thin film has a modulation depth of ~2% and a saturable fluence of 10.6 μJ/cm^2. CNT-PVA thin film has a modulation depth of ~4.5% and a saturable fluence of 6.8 μJ/cm^2. There are also ~20% non-saturable loss in each thin film which is probably due to the PVA absorption and scattering loss. As a reference, the saturable absorption of the SESAM (BATOP SAM-1550-9-2ps) is also measured. It has a modulation depth of ~6% and a saturable fluence of 40.2 μJ/cm^2. The fitting curves based a two-level SA model are also plotted in Fig. 2. Two-photon absorption effect is considered for the SESAM in the fitting.

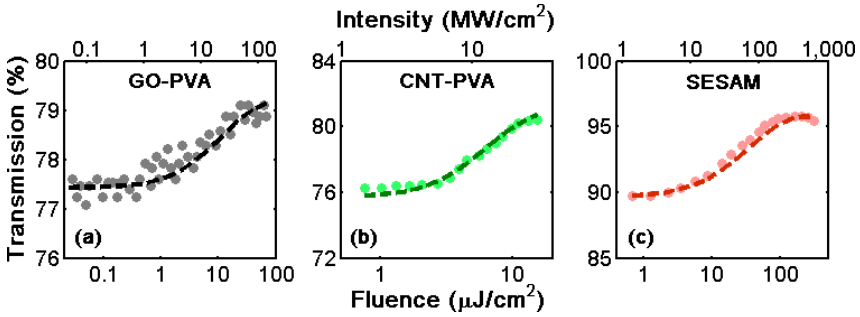

Fig. 2. Modulation depth of (a) GO-PVA thin film, (b) CNT-PVA thin film and (c) SESAM.

3. Experimental setup and laser optical properties

In order to compare the mode locking operation and the timing phase noise properties of different SAs, a fiber laser is designed as shown in Fig. 3(a). The laser has a linear cavity. The left cavity mirror is a partial reflection coating with 90% reflection at 1550 nm. The cavity consists of a 25-cm Erbium-doped fiber (EDF, Er 110 4/125) with normal dispersion of −8 ps/km·nm and ~135 cm standard single mode fiber with anomalous dispersion of 17 ps/km·nm. The net dispersion is ~21 fs/nm. The SAs are placed at the right side of the cavity. For GO-PVA and CNT-PVA thin films, they are embedded between a fiber end and a total reflection mirror coating (on another fiber end), shown in Fig. 3(b). For SESAM, it is directly butt coupled to the fiber end. 976-nm pump is injected into the cavity through a 980/1550 wavelength division multiplexer (WDM) outside the cavity. Different SAs share the same laser cavity to exclude the influence of laser cavity difference and thus the laser output can actually reflect the role of these SAs on the mode locking operation and laser timing phase noise. The output of the laser is fed into the measurement equipment including optical spectrum analyzer (OSA), autocorrelator and signal source analyzer (R&S FSUP26) for the characterization of its optical and noise properties. Pump modulation technique is applied to measure the noise conversion from the pump RIN to the laser noise, which will be discussed in detail later.

#224095 - $15.00 USD Received 29 Sep 2014; revised 7 Nov 2014; accepted 10 Nov 2014; published 9 Jan 2015

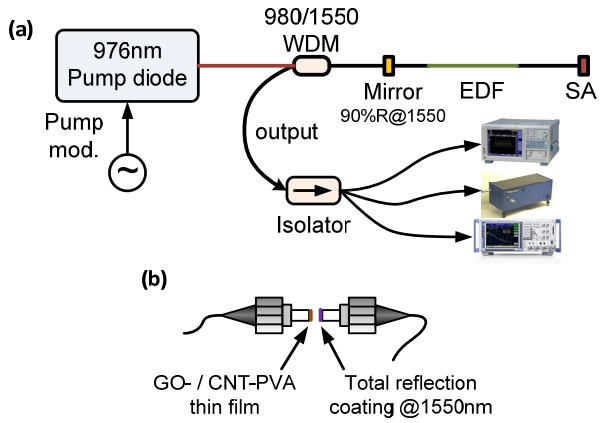

Fig. 3. (a) Laser design with a linear cavity; (b) Placement of GO-PVA and CNT-PVA thin film saturable absorbers.

The general optical properties of three mode-locked lasers are summarized in Table 1.

Table 1. Optical properties of the mode-locked lasers

	GO laser	CNT laser	SESAM laser
Pump power	131 mW	92 mW	163 mW
Output power	820 μW	445 μW	1.3 mW
Center wavelength	1561.8 nm	1560.1 nm	1563.2 nm
3-dB bandwidth	4.7 nm	4.3 nm	6.2 nm
Pulse width	735 fs	763 fs	709 fs
Rep. rate	62.2 MHz	62.2 MHz	62.2 MHz

It can be observed that CNT laser has the lowest pump power and output power, which is consistent with its low saturation intensity. GO laser has a higher pump power and output power due to the higher saturation intensity. For comparison, SESAM laser has the highest output power due to the highest saturation intensity and the lowest non-saturable loss.

4. Laser noise properties

To compare the timing phase noise properties of the lasers, we first describe the noise coupling mechanisms from the pump to the lasers, shown in Fig. 4. Pump RIN directly couples to the laser RIN via the modulation of the gain media [10, 52]. This noise conversion ratio is denoted as r_{RIN}. Laser RIN then couples to the laser phase noise via fiber nonlinearity and SSA effect, denoted as Δr_{PN} [51]. SSA effect means the saturation of the absorber is not instant. Therefore the rising edge and the falling edge of the input pulse will experience different loss which leads to the tilting of the pulse shape and the shift of the pulse timing. Pump RIN can also directly couples to the laser phase noise via thermal effect and nonlinearity [55]. The total noise conversion ratio from the pump RIN to the laser phase noise is denoted as r_{PN}, including both the direct coupling (Pump RIN → Laser phase noise) and indirect coupling (Pump RIN → Laser RIN → Laser phase noise).

#224095 - $15.00 USD Received 29 Sep 2014; revised 7 Nov 2014; accepted 10 Nov 2014; published 9 Jan 2015

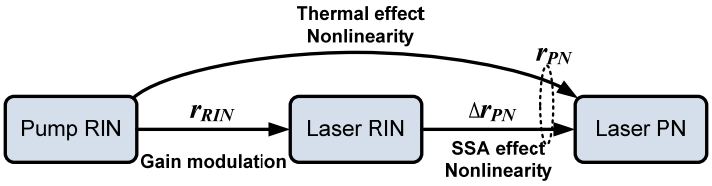

Fig. 4. Noise coupling from the pump to the laser and inside the laser. SSA: slow saturable absorber; RIN: relative intensity noise; PN: phase noise.

In the experiment, r_{RIN} and r_{PN} are measured by using pump modulation technique. Through applying a weak modulation to the pump drive current, a spurious peak at the modulation frequency f_M can be generated in the pump RIN spectrum. This pump RIN couples to the laser noise and generates spurious peaks at the same frequency f_M in the laser RIN and phase noise spectra. By comparing the power difference of the spurious peaks between the laser noise spectrum and the pump RIN spectrum, r_{RIN} and r_{PN} at frequency f_M are obtained. Then tuning the modulation frequency f_M from 100 Hz to 80 kHz, the frequency dependence of r_{RIN} and r_{PN} can also be obtained. The noise conversion from the laser RIN to the laser phase noise (Δr_{PN}) can't be experimentally measured. Instead, we use theoretical model to estimate it.

For GO laser, the measured laser RIN and phase noise spectra are shown in Fig. 5(a). The pump RIN spectrum is shown in the inset. The corresponding noise conversion ratios are shown in Fig. 5(b). The calculated laser RIN and phase noise spectra in Fig. 5(a) are obtained using the following relations

$$S_{cal} = S_{Pump-RIN} \cdot r \tag{1}$$

where S_{cal} represents the calculated laser RIN or phase noise spectrum, $S_{Pump\text{-}RIN}$ is the pump RIN spectrum and r represents the measured noise conversion ratio r_{RIN} or r_{PN}. Very good agreement at low offset frequency can be found in Fig. 5(a). The deviation at high offset frequency is due to the noise floor of the measurement system. This result suggests that the measured noise conversion ratios are able to represent the noise properties in the laser operation.

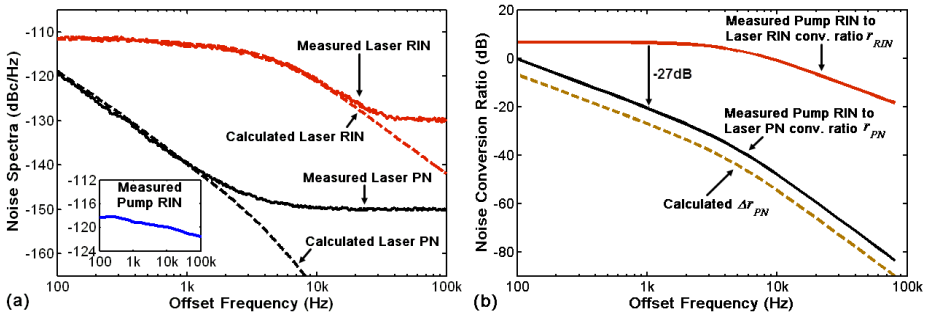

Fig. 5. (a) Noise spectra of the GO laser. Inset: Pump RIN spectrum; (b) Measured noise conversion ratios and calculated excess phase noise conversion Δr_{PN} due to the SSA effect.

We have previously shown that SSA effect is the dominant effect causing laser RIN to laser phase noise coupling in a linear cavity when we refer to the *absolute* timing phase noise [52]. Therefore we can use the theoretical model of SSA to estimate Δr_{PN}, given by [51]

$$\Delta S_{PN}(f) = \left(\frac{f_R^2}{f} \frac{\partial \Delta t}{\partial s} s \right)^2 S_{RIN}(f) \tag{2}$$

#224095 - $15.00 USD Received 29 Sep 2014; revised 7 Nov 2014; accepted 10 Nov 2014; published 9 Jan 2015

$$\Delta r_{PN}(f) = \left(\frac{f_R^2}{f} \frac{\partial \Delta t}{\partial s} s \right)^2 r_{RIN}(f) \tag{3}$$

where ΔS_{PN} is the excess phase noise coupled from the laser RIN, f_R is the repetition rate, f is the offset frequency, s is the saturation parameter defined as the ratio between input pulse energy and the SA saturation energy, Δt is the pulse temporal shift due to the SSA effect. It can be seen that the material properties and the laser operation specifications have been included in the SSA model. The calculation of $\partial \Delta t/\partial s$ implements the differential equation governing the SSA, given by [56]

$$\frac{\partial q}{\partial t} = \frac{q_m - q}{\tau_A} - q \frac{P(t)}{E_A} \tag{4}$$

where q is the instant SA absorption, q_m is the modulation depth, τ_A is the SA decay time, $P(t)$ is the instant power of the pulse and E_A is the SA saturation energy. The calculated pulse temporal shift Δt with respect to s is shown in Fig. 6. For an easy comparison, the modulation depths for different SAs are all normalized to 1%. The temporal shift is proportional to the modulation depth for a given s. Using a homemade pump-probe system, the decay time of GO and CNT is measured, shown in Fig. 7. The laser source in the pump-probe system is a Ti:Sapphire mode-locked laser centered at 800 nm with a pulse width of 100 fs (Spectra-Physics Tsunami Series). The fast decay time of GO and CNT is measured to be 380 fs and 560 fs, respectively which is close to the measured values reported in other works [57, 58]. The relaxation in the GO and CNT originates from two effects: the ultrafast intraband relaxation corresponding to a decay time of a few hundreds of femtosecond and the slower interband relaxation corresponding to a decay time of picosecond level. The decay time of SESAM is estimated to be 2 ps [59]. It can be seen that, GO has the most flat curve due to its small decay time and SESAM has the sharpest curve due to its long decay time. This indicates that the laser RIN to phase noise conversion induced by SSA effect should be weakest in the GO laser and strongest in the SESAM laser. One may find that for a saturation parameter s near 3, the slope $\partial \Delta t/\partial s$ becomes zero which means an elimination of the noise conversion. However, the actual value for s in many experimentally reported mode-locked lasers are far beyond this value (typically $s > 6$) due to the fact that SAs are usually deeply saturated in the mode locking operation [53, 60]. Moreover, even the mode locking is obtained for $s = 3$, the laser output power is sacrificed because s is defined as the ratio between pulse energy and SA saturation energy, and most probably the output bandwidth will also be reduced due to the lower pulse energy. For the SA with even longer decay time (i.e., sufficiently larger than the pulse width), the temporal shift will increase very weakly and the noise conversion reaches a constant value.

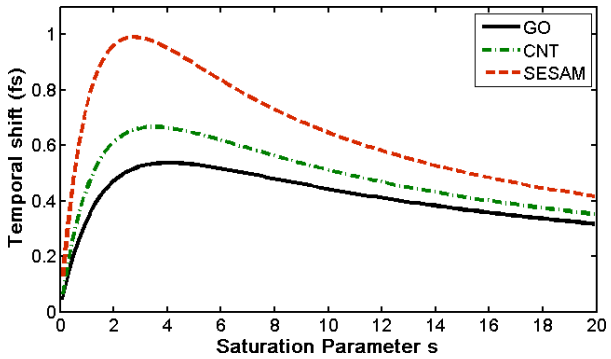

Fig. 6. Pulse temporal shift induced by the slow saturable absorber effect with 1% modulation depth.

#224095 - $15.00 USD Received 29 Sep 2014; revised 7 Nov 2014; accepted 10 Nov 2014; published 9 Jan 2015

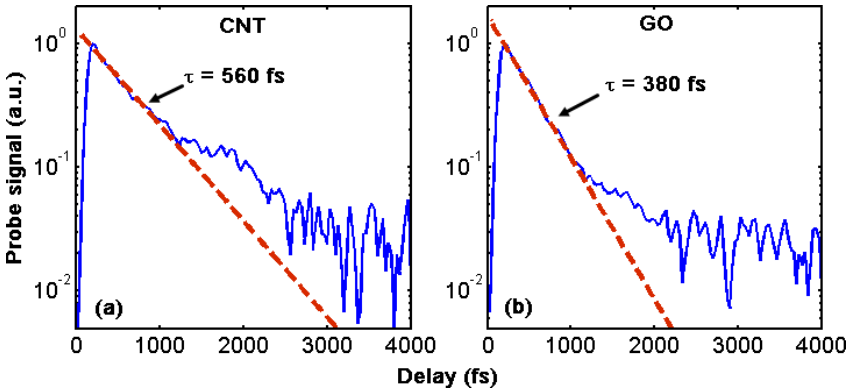

Fig. 7. Decay time of (a) CNT and (b) GO.

It should also be mentioned that nanomaterials usually exhibit two decay timescales due to the fast intraband relaxation and slow interband relaxation [12, 61]. Although such a decay model with two time constants cannot be modelled using the form of differential equation in Eq. (4), we can still perform an approximate analysis. Using CNT as an example, its two decay time constants are τ_1 = 560 fs and τ_2 = 1.2 ps. The decay time can be expressed by

$$decay = \exp\left(-\frac{t}{\tau_1}\right) + 0.361\exp\left(-\frac{t}{\tau_2}\right) \tag{5}$$

where the coefficient 0.361 represents the strength of the slow interband relaxation. The equation can be re-written as

$$decay = \exp\left(-\frac{t}{\tau_1}\right) + \exp\left(-\frac{t-1.22\,ps}{\tau_2}\right) \tag{6}$$

Equation (6) means the strength of slow relaxation is comparable to the fast relaxation after 1.22 ps. Note that for most low-jitter mode-locked lasers, pulse width is much shorter than this time. Therefore, it can be inferred that the influence of slow decay time is negligible.

We use the following values for the calculation of Δr_{PN} in Eq. (7) for the GO laser: f_R = 62.2 MHz, s = 17.1 and $\partial\Delta t/\partial s$ = 0.16 fs. It can be seen that the calculated Δr_{PN} nearly has identical trend compared with the measured r_{PN} except for a 6-dB vertical shift in Fig. 5(b). The shift is attributed to the error in the estimation of material decay time and temporal shift. There is no other mechanism which leads to an f^{-2} dependence on the laser RIN. Therefore this result demonstrates that SSA effect is the dominant effect causing laser RIN to phase noise conversion in the GO laser.

$$\Delta r_{PN}(f) = r_{RIN}(f) - 20\lg f + 26.5\ (\text{dB}) \tag{7}$$

Similarly, the noise spectra and the noise conversion ratios for the CNT laser and the SESAM laser are also measured, shown in Fig. 8 and Fig. 9. Again, the laser RIN and phase noise can be estimated by using the measured pump RIN spectrum and the noise conversion ratios. Good agreement between the measured noise spectra and the calculated noise spectra can be observed. We use the following values for the calculation of Δr_{PN} in Eq. (8) for the CNT laser: f_R = 62.2 MHz, s = 13 and $\partial\Delta t/\partial s$ = 0.16 fs. And the following values in Eq. (9) for the SESAM lasers: f_R = 62.2 MHz, s = 6.5 and $\partial\Delta t/\partial s$ = 0.3 fs.

$$\Delta r_{PN}(f) = r_{RIN}(f) - 20\lg f + 31.2\ (\text{dB}) \tag{8}$$

$$\Delta r_{PN}(f) = r_{RIN}(f) - 20\lg f + 33.1\ (\text{dB}) \tag{9}$$

#224095 - $15.00 USD Received 29 Sep 2014; revised 7 Nov 2014; accepted 10 Nov 2014; published 9 Jan 2015

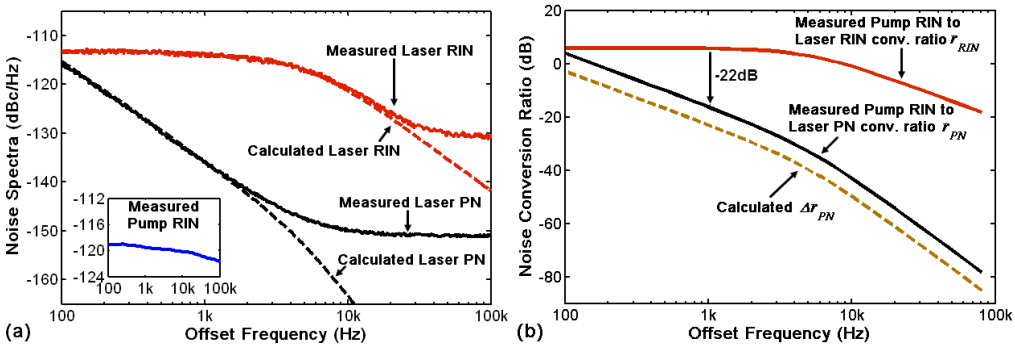

Fig. 8. (a) Noise spectra of the CNT laser. Inset: Pump RIN spectrum; (b) Measured noise conversion ratios and calculated excess phase noise conversion Δr_{PN} due to the SSA effect.

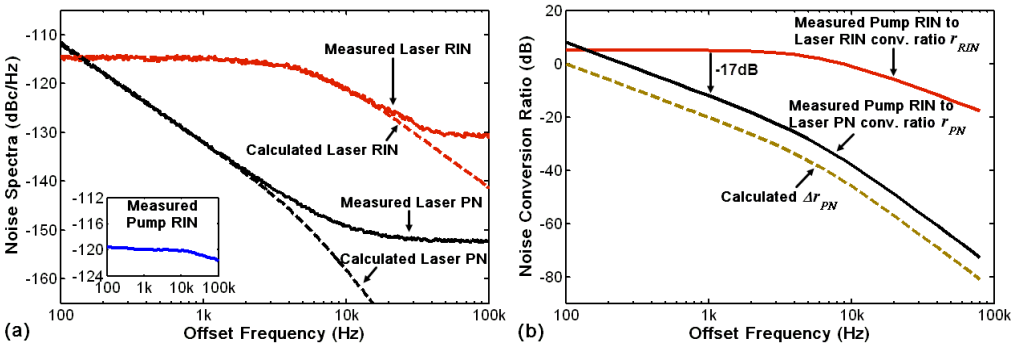

Fig. 9. (a) Noise spectra of the SESAM laser. Inset: Pump RIN spectrum; (b) Measured noise conversion ratios and calculated excess phase noise conversion Δr_{PN} due to the SSA effect

As expected, due to the smallest material decay time of GO, the GO laser shows the lowest timing phase noise, lowest pump RIN to laser phase noise conversion ratio r_{PN} and lowest Δr_{PN} induced by the SSA effect. In comparison, all these noise parameters in the CNT laser are higher than those in the GO laser, which is consistent with the fact that CNT has larger material decay time than GO. Moreover, due to the largest decay time in SESAM, the SESAM laser exhibits the highest noise properties among three lasers. For a more clear comparison on the timing phase noise of three lasers, the noise properties are summarized in Table 2. The minimum measureable timing jitter is ~11.4 fs at the repetition rate limited by the noise floor of the signal source analyzer and the shot noise. It can be seen that compared with the SESAM laser, the GO laser has a phase noise conversion 8.6 dB lower at 1 kHz, a phase noise 7 dB lower at 1 kHz and a timing jitter 45% reduced integrated from 100 Hz to 100 kHz while CNT laser has a phase noise conversion 4.3 dB lower, a phase noise 3 dB lower and a timing jitter 29% reduced.

However, it must also be clarified that our results do not reach the conclusion that SESAM is not a good SA compared with GO and CNT. In fact, from the view of optical properties the SESAM laser has the widest spectrum and the highest output power under the same laser cavity configuration, which benefits from its low non-saturable loss and high saturable fluence. Reducing the non-saturable loss and increasing the saturable fluence are still challenging in the preparation of GO and CNT SAs. But meanwhile, nanomaterials SAs such as graphene, GO and CNT have the advantages of broadband operation, i.e., a single SA can be used in a wide range of operation wavelength from visible to mid-IR while a SESAM can only be used for a specific wavelength.

It is worth mentioning that graphene in principle should give smaller phase noise conversion due to its very fast decay time and thus very weak SSA effect. Also, the fastest SA is the mode locking based on fiber nonlinearity, or NPE (nonlinear polarization evolution).

#224095 - $15.00 USD Received 29 Sep 2014; revised 7 Nov 2014; accepted 10 Nov 2014; published 9 Jan 2015

And it has been experimentally confirmed that the laser mode locked by NPE has much weaker SSA induced noise conversion in our previous work [52].

Table 2. Noise properties of the three lasers

	GO laser	CNT laser	SESAM laser
Phase noise conversion at 1kHz	−20.6 dB	−16.3 dB	−12.0 dB
Phase noise at 1kHz	−139 dBc/Hz	−136 dBc/Hz	−132 dBc/Hz
Timing jitter (100Hz-100kHz)	52.9 fs	67.8 fs	95.8 fs

4. Conclusion

In conclusion, the timing phase noise properties of mode-locked lasers are characterized and compared when three different saturable absorbers GO, CNT and SESAM are utilized. Three saturable absorbers share exactly the same linear laser cavity so that the influence of the cavity difference is excluded and the laser output can actually reflect the role of these saturable absorbers on the laser timing phase noise. It is found that due to the smaller saturable absorber decay time and thus weaker excess phase noise conversion induced by the slow saturable absorber effect, both the GO laser and the CNT laser exhibit better timing phase noise and timing jitter compared with the SESAM laser. A timing phase noise reduction of 7 dB and a timing jitter reduction of 45% are achieved in the GO laser. And a timing phase noise reduction of 3 dB and a timing jitter reduction of 29% are achieved in the CNT laser. Moreover, the method presented in this paper can be applied to any other saturable absorbers to investigate their timing noise properties. Our finding suggests that saturable absorbers with fast decay time may have the potential for low-timing-phase-noise mode locking operation.

Acknowledgments

This work is partially supported by Shanghai Yangfan program (No. 14YF1401600), the State Key Lab Project of Shanghai Jiao Tong University (No. GKZD030033), A*STAR SERC grant (No. 112-290-4018) and A*STAR SERC Advanced Optics in Engineering Programme (No. 122-360-0004).

#224095 - $15.00 USD Received 29 Sep 2014; revised 7 Nov 2014; accepted 10 Nov 2014; published 9 Jan 2015